PNAS RESEARCH ARTICLE | ENVIRONMENTAL SCIENCES

Climate change determines the sign of productivity trends in US forests

J. Aaron Hogan[a,1], Grant M. Domke[b], Kai Zhu[c], Daniel J. Johnson[d], and Jeremy W. Lichstein[a]

Edited by Donald Ort, University of Illinois at Urbana Champaign, Urbana, IL; received July 21, 2023; accepted December 1, 2023

Forests are integral to the global land carbon sink, which has sequestered ~30% of anthropogenic carbon emissions over recent decades. The persistence of this sink depends on the balance of positive drivers that increase ecosystem carbon storage—e.g., CO_2 fertilization—and negative drivers that decrease it—e.g., intensifying disturbances. The net response of forest productivity to these drivers is uncertain due to the challenge of separating their effects from background disturbance–regrowth dynamics. We fit non-linear models to US forest inventory data (113,806 plot remeasurements in non-plantation forests from ~1999 to 2020) to quantify productivity trends while accounting for stand age, tree mortality, and harvest. Productivity trends were generally positive in the eastern United States, where climate change has been mild, and negative in the western United States, where climate change has been more severe. Productivity declines in the western United States cannot be explained by increased mortality or harvest; these declines likely reflect adverse climate-change impacts on tree growth. In the eastern United States, where data were available to partition biomass change into age-dependent and age-independent components, forest maturation and increasing productivity (likely due, at least in part, to CO_2 fertilization) contributed roughly equally to biomass carbon sinks. Thus, adverse effects of climate change appear to overwhelm any positive drivers in the water-limited forests of the western United States, whereas forest maturation and positive responses to age-independent drivers contribute to eastern US carbon sinks. The future land carbon balance of forests will likely depend on the geographic extent of drought and heat stress.

aboveground biomass | forest productivity | growth enhancement | stand maturation | climate change

Significance

Increases in forest carbon storage have slowed climate change over recent decades, but the future of this carbon sink is uncertain. The net forest carbon sink is determined by the balance between positive drivers (e.g., the enhancement of photosynthesis due to rising concentrations of atmospheric CO_2) and negative drivers (e.g., increasing frequency and intensity of drought and wildfire). From ~1999 to 2020, forest productivity increased in much of the eastern United States, where mild warming was accompanied by mild increases in precipitation. In contrast, forest productivity decreased in much of the western United States, where warming was more severe, and precipitation declined. These results highlight the vulnerability of the global forest carbon sink to climate change.

The land carbon sink has offset ~25 to 30% of global anthropogenic carbon emissions over recent decades, providing an essential ecosystem service that slows climate change (1, 2). However, there is considerable uncertainty in the future land–atmosphere carbon balance (3, 4). Much of the land sink is thought to reside in forests (5, 6). Some empirical studies suggest weakening forest carbon sinks due to warming, water stress, and intensifying disturbance regimes (7, 8), whereas most Earth system models (ESMs) predict a persistent land carbon sink due to the positive effects of rising atmospheric CO_2 concentrations on photosynthesis and ecosystem carbon storage ("CO_2 fertilization") (4). The strength and stability of forest carbon sinks depend on the net effect of multiple drivers (8), including both positive drivers [e.g., CO_2 fertilization and nitrogen deposition (9, 10)] and negative drivers [e.g., intensifying disturbance regimes (11, 12)].

Some studies indicate an important role for CO_2 fertilization in the global forest carbon sink (13–15), but other studies provide ambiguous or contradictory evidence (16). Leaf photosynthesis responds strongly to increases in CO_2 at near-instantaneous timescales (17, 18), but multiple factors may constrain how leaf-level responses translate to tree-level biomass production and ecosystem carbon storage (16). These constraining factors include CO_2-induced changes in respiration rates and tree carbon allocation (16, 19–21), as well as water and nutrient limitations (22, 23). For CO_2 fertilization to contribute to forest carbon sinks, leaf-level responses must translate to increases in carbon storage in live trees (biomass) or other ecosystem carbon pools (e.g., litter and soil) (16, 22). Free-air CO_2-enrichment experiments in young forests show a ~30% increase in the rate of tree biomass production over the first decade (24), but this effect usually attenuates over time (25, 26). Thus, the prevalence, strength, and persistence of CO_2 fertilization on forest productivity (the rate of biomass production) and carbon storage remain uncertain (16). CO_2 fertilization is expected to be strongest under conditions that support high productivity (moderate temperatures and sufficient water and nutrients) (25, 26), and changes in these non-CO_2 factors may also directly contribute to forest carbon sinks (16, 21, 22). However, the effects of CO_2 fertilization or other positive drivers of forest carbon storage may be overwhelmed in some cases by negative drivers (8, 11).

Author contributions: J.A.H., G.M.D., and J.W.L. designed research; J.A.H., G.M.D., K.Z., D.J.J., and J.W.L. performed research; J.A.H. analyzed data; and J.A.H., G.M.D., K.Z., D.J.J., and J.W.L. wrote the paper.

The authors declare no competing interest.

This article is a PNAS Direct Submission.

[1]To whom correspondence may be addressed. Email: hogan.jaaron@ufl.edu.

This article contains supporting information online at https://www.pnas.org/lookup/suppl/doi:10.1073/pnas.2311132121/-/DCSupplemental.

Published January 16, 2024.

Negative drivers that can decrease forest productivity and carbon storage include increases in the frequency or intensity of disturbance—e.g., fire, drought, insect outbreaks, and timber harvest (11, 27–29). Intensifying disturbance regimes are impacting many forested regions of the globe because of the coupled and often compounding effects of multiple drivers and their interaction with changing climates (11, 30). As a result, rates of tree mortality are increasing (31, 32), which directly reduces carbon storage in live trees and can also cause productivity declines by reducing the growing stock (live biomass). Additionally, decreases in tree growth rates due to climatic stress—especially in water-limited forest ecosystems or where trees are near thermal thresholds—likely contribute to forest biomass declines (29, 33–35). Thus, negative drivers can reduce forest productivity both through increased tree mortality and through decreased tree growth rates.

US forests provide a valuable test case for studying the balance of positive and negative drivers of productivity trends because there are standardized national forest inventories spanning multiple decades (36) and large geographic variations in historical climate and recent climate change (37). An analysis of forest inventory data from five eastern US states from the late-1970s to mid-1990s revealed no significant productivity trends, leading to the conclusion that the US forest sink was due solely to regrowth from previous land use (38). In contrast, a more recent study of eastern US forests (39) reported a CO_2 fertilization-attributable increase in wood volume (0.35% y^{-1}) from 1970 to 2015. US forests are currently a net carbon sink on average—offsetting ~13% of US annual greenhouse gas emissions—but there is wide regional variation in the sign and magnitude of US forest carbon fluxes (40). Beyond the uncertain effects of CO_2 fertilization, ongoing recovery from industrial logging and agricultural abandonment are widely accepted as contributing to a carbon sink in the eastern United States (27, 38, 41, 42), whereas intensifying disturbance regimes likely contribute to negative carbon balances in some western states (28, 40). The role of productivity trends—alone, or in combination with mortality trends (29, 31)—in determining the carbon balance of US forests is unknown.

We used national-scale forest inventory data—comprising 113,806 remeasurements of 57,532 plot locations in non-plantation forests across the coterminous United States from ~1999 to 2020—to estimate productivity trends (τ; $\%y^{-1}$) for different ecoprovinces (*SI Appendix*, Fig. S1) while controlling for biomass losses due to mortality and harvest. We chose the ecoprovince scale for our analyses because ecoprovinces represent areas with similar climate, soil, and potential natural vegetation (43) that are big enough to provide large sample sizes (>1,000 remeasured inventory plots in most cases; Table 1). Analyses of broader geographic units would increase noise (due to heterogeneity in environmental conditions) and potential bias (differences in the timing of sampling among US states that may differ in productivity), whereas analyses of smaller geographic units are unlikely to provide sufficient sample sizes to detect productivity trends.

To aid in identifying robust trends, we consider models of both stand-level tree carbon storage ("biomass stock": aboveground dry wood biomass of live trees, Mg ha^{-1}, where ~50% of wood dry mass is carbon) and stand-level biomass production ("biomass growth": production rate of aboveground dry wood biomass, Mg ha^{-1} y^{-1}), and we consider model forms both with and without stand age (the mean age of trees in the dominant size class; 44) as a predictor variable. Specifically, we considered three model forms, all of which estimate the productivity trend (τ) by including year as a predictor variable (*SI Appendix*, Fig. S2): 1) biomass stock as a function of stand age and year, 2) biomass growth as a function of stand age and year, and 3) biomass growth as a function of biomass stock and year. A positive (or negative) τ indicates a positive (or negative) temporal trend in biomass stock or growth that cannot be explained by other model terms (i.e., biomass losses and either stand age or biomass stock, depending on the model form). Positive τ implies that positive drivers (e.g., CO_2 fertilization) have stronger temporal effects than negative drivers, and negative τ implies the reverse. To evaluate the robustness of our results, we analyze different data subsets to control for the number of remeasurements per plot location or to exclude plot locations with any reported harvest. (Although our analyses were restricted to non-plantation forests, selective or clear-cut harvesting occurs in many naturally regenerating forests in the United States).

We use our modeling framework to quantify how productivity trends vary across ecoprovinces that have experienced variable signs and magnitudes of climate change, ranging from increased precipitation and mild warming in parts of the eastern United States to decreased precipitation and greater warming in parts of the western United States. In addition, we leverage the large number of eastern US plots that have been inventoried at least three times to partition changes in biomass stocks into stand-age-dependent and age-independent components, thereby providing insights into the causes of the eastern US forest carbon sink.

1. Results

1.1. Productivity Trends in Non-Plantation Forests of the Coterminous United States. Productivity trend (τ) estimates were mostly positive or non-significant in eastern US ecoprovinces but negative or non-significant in western US ecoprovinces (Fig. 1*A*). Mean productivity trends were significantly positive in the eastern United States and significantly negative in the western United States (*SI Appendix*, Fig. S3). Within ecoprovinces, τ estimates were mostly consistent across the three model forms (Fig. 1*B* and *SI Appendix*, Table S1). These results were robust to temporal variation in the location of inventory plots and to the effects of harvesting. Specifically, fitting the models to filtered datasets with a temporally balanced design (which was restricted to plot locations measured at least three times, and which represented each of these plots by two remeasurement intervals) or that excluded plot locations with any reported harvest led to similar results (*SI Appendix*, Fig. S4 and Table S1).

1.2. Productivity Trends in Relation to Climate Change. Across ecoprovinces, productivity trends (τ) tended to be positive in ecoprovinces that experienced increased water availability and mild warming over recent decades (as in much of the eastern United States) and tended to be negative in ecoprovinces that experienced decreased water availability and more pronounced warming (as in much of the western United States; Fig. 2 and *SI Appendix*, Fig. S5). Specifically, across ecoprovinces, τ increased with increasing ecosystem water balance (as measured by change-over-time in the Palmer Drought Severity Index) and increasing precipitation change; and τ decreased with increasing climate warming (Fig. 2). Productivity trends tended to be negative in ecoprovinces that have warmed faster than ~0.02 C y^{-1} over recent decades (Fig. 2).

1.3. Age-Dependent and Age-Independent Components of Biomass Change in the Eastern United States. Our modeling framework, along with the large sample of eastern US plot locations inventoried three or more times (two or more remeasurements), allowed us to partition observed changes in aboveground biomass stocks ($\Delta B_{observed}$) in eastern US ecoprovinces into stand age-, productivity trend-, and disturbance-related components. The sum of the three modeled components closely matched the

Table 1. Sample size and climate variables for United States ecoprovinces

			Plot remeasurements (*n*)			Ecosystem water balance		Precipitation		Temperature	
Region	Code	Ecoprovince name	Pre-2010	Post-2010	Total	PDSI	ΔPDSI (y^{-1})	MAP (mm)	ΔMAP (mm y^{-1})	MAT(°C)	ΔMAT (°C y^{-1})
Eastern United States	231	Southeastern Mixed Forest	5,042	7,802	12,844	0.95 ± <0.01	−0.002 ± <0.001	1,341 ± 1	1.47 ± 0.01	16.32 ± 0.01	0.0171 ± 0.0001
	232	Outer Coastal Plain Mixed Forest	4,528	8,639	13,167	0.64 ± <0.01	−0.013 ± <0.001	1,349 ± 1	2.38 ± 0.02	18.39 ± 0.02	0.0115 ± 0.0001
	M221	Central Appalachian Broadleaf Forest—Coniferous Forest—Meadow	2,863	5,323	8,186	0.88 ± <0.01	0.003 ± <0.001	1,307 ± 3	1.30 ± 0.02	11.30 ± 0.02	0.0179 ± 0.0001
	211	Northeastern Mixed Forest	2,371	4,513	6,884	1.44 ± <0.01	0.028 ± <0.001	1,154 ± 1	1.89 ± 0.01	6.62 ± 0.01	0.0220 ± 0.0001
	M211	Adirondack-New England Mixed forest—Coniferous Forest—Alpine Meadow	1,887	4,891	6,778	1.37 ± <0.01	−0.003 ± <0.001	1,203 ± 2	0.69 ± 0.02	4.75 ± 0.02	0.0225 ± 0.0001
	M231	Ouachita Mixed Forest	182	827	1,009	1.21 ± 0.01	0.009 ± <0.001	1,392 ± 4	2.75 ± 0.05	15.87 ± 0.01	0.0090 ± 0.0001
	212	Laurentian Mixed Forest	12,252	10,433	22,685	1.01 ± <0.01	0.022 ± <0.001	784 ± 1	1.45 ± 0.01	4.69 ± 0.01	0.0138 ± <0.0001
	234	Lower Mississippi Riverine Forest	233	1,111	1,344	1.13 ± 0.01	0.008 ± <0.001	1,427 ± 3	1.65 ± 0.05	17.61 ± 0.04	0.0152 ± 0.0001
	251	Temperate Prairie Parkland	1,170	1,120	2,290	1.21 ± <0.01	0.039 ± <0.001	951 ± 2	2.53 ± 0.02	10.89 ± 0.04	0.0095 ± 0.0001
	222	Midwest Broadleaf Forest	2,970	2,876	5,846	1.46 ± <0.01	0.056 ± <0.001	880 ± 1	3.08 ± 0.01	7.66 ± 0.02	0.0158 ± 0.0001
	221	Eastern Broadleaf Forest	2,405	4,902	7,307	1.22 ± <0.01	0.023 ± <0.001	1,228 ± 2	2.27 ± 0.02	11.03 ± 0.02	0.0201 ± 0.0001
	223	Central Interior Broadleaf Forest	4,948	5,058	10,006	1.27 ± <0.01	0.032 ± <0.001	1,233 ± 1	3.02 ± 0.01	13.49 ± 0.01	0.0154 ± 0.0001
	M223	Ozark Broadleaf Forest Meadow	231	662	893	0.91 ± <0.01	0.019 ± <0.001	1,321 ± 3	2.59 ± 0.05	14.51 ± 0.02	0.0105 ± 0.0001
	255	Subtropical Prairie Parkland	244	490	714	1.13 ± 0.01	0.002 ± <0.001	1,128 ± 3	2.83 ± 0.04	10.28 ± 0.06	0.0171 ± 0.0003
Western United States	M333	Northern Rocky Mountain Steppe—Coniferous Forest—Alpine Meadow	16	1,742	1,758	0.15 ± 0.01	−0.038 ± <0.001	927 ± 9	−1.36 ± 0.04	5.21 ± 0.04	0.0231 ± 0.0002
	M332	Southern Rocky Mountain Steppe—Open Woodland—Coniferous Forest—Alpine Meadow	0	1,757	1,757	0.26 ± 0.01	0.058 ± <0.001	719 ± 5	−1.11 ± 0.04	3.24 ± 0.05	0.0311 ± 0.0002
	332	Great Plains Steppe	78	154	232	1.44 ± 0.02	0.057 ± 0.001	619 ± 7	2.36 ± 0.06	9.27 ± 0.21	0.0089 ± 0.0004
	M334	Black Hills Coniferous Forest	214	237	451	1.20 ± 0.01	0.021 ± 0.001	566 ± 4	1.74 ± 0.02	6.13 ± 0.07	0.0210 ± 0.0003
	M331	Southern Rocky Mountain Steppe—Open Woodland—Coniferous Forest—Alpine Meadow	0	1,757	1,757	0.46 ± 0.01	−0.042 ± 0.001	719 ± 5	−1.11 ± 0.04	3.24 ± 0.05	0.0311 ± 0.0002
	313	Colorado Plateau Semi-Desert	0	218	218	0.13 ± 0.02	−0.083 ± 0.002	555 ± 10	−2.59 ± 0.10	7.68 ± 0.13	0.0320 ± 0.0007
	331	Great Plains/Palouse Dry Steppe	61	270	331	0.89 ± 0.03	0.050 ± 0.002	472 ± 7	1.10 ± 0.07	7.79 ± 0.07	0.0123 ± 0.0004
	M341	Nevada-Utah Mountains Semi-Desert—Coniferous Forest—Alpine Meadow	0	220	220	0.34 ± 0.02	−0.023 ± 0.001	611 ± 10	−0.84 ± 0.08	4.69 ± 0.11	0.0271 ± 0.0007
	M313	Arizona-New Mexico Mountains Semi-Desert—Open Woodland—Coniferous Forest—Alpine Meadow	0	367	367	−0.04± 0.02	−0.085 ± 0.002	637 ± 7	−3.27 ± 0.07	8.57 ± 0.09	0.0383 ± 0.0006
	M242	Cascade Mixed Forest	22	3,281	3,303	0.15 ± 0.01	−0.041 ± <0.001	1,590 ±16	−1.28 ± 0.05	7.12 ± 0.04	0.0190 ± 0.0002
	M261	Sierran Steppe—Mixed Forest—Coniferous Forest—Alpine Meadow	202	1,791	1,993	−0.19 ± 0.01	−0.050 ± <0.001	1,247 ± 12	−1.50 ± 0.04	9.35 ± 0.05	0.0307 ± 0.0003

The number of plot remeasurements used in our analysis is given. Inventory records were assigned to the pre- or post-2010 period based on the remeasurement date. Climate variables are ecosystem water balance (Palmer Drought Severity Index, PDSI; unitless; higher values indicate wetter conditions), mean annual precipitation (MAP), and mean annual temperature (MAT). For each climate variable, we report its 50-y (1972 to 2022) mean (±SE) and its change (Δ; 50-y trend ± SE). See *SI Appendix*, Fig. S1 for a map of ecoprovince codes.

$\Delta B_{observed}$ values (*SI Appendix*, Fig. S6*A*), which were significantly positive for 13 of 14 eastern US ecoprovinces (Fig. 3*A*). Stand age distributions shifted toward older ages in all 14 ecoprovinces (Fig. 3*B*), and biomass change due to changes in stand age (ΔB_{age}) was significantly positive for 13 or 14 ecoprovinces (Fig. 3*A*). Biomass change due to productivity trends ($\Delta B_{productivity\ trend}$) was significantly positive for 8 of 14 ecoprovinces (Fig. 3*A*). In contrast, biomass change due to changes in mortality and harvest losses ($\Delta B_{disturbance}$) was significantly negative in 12 of 14 ecoprovinces (Fig. 3*A*). As expected, ΔB_{age} tended to be large in ecoprovinces with large increases in mean stand age (*SI Appendix*, Fig. S6*B*), $\Delta B_{productivity\ trend}$ was strongly determined by τ (*SI Appendix*, Fig. S6*C*), and $\Delta B_{disturbance}$ was strongly determined by mortality and harvest effects (*SI Appendix*, Fig. S6*D*). The magnitudes of ΔB_{age} and $\Delta B_{productivity\ trend}$ were roughly equal to each other (means of 0.65 and 0.58 Mg ha^{-1} y^{-1}, respectively, across ecoprovinces) and larger than that of $\Delta B_{disturbance}$ (mean of −0.22 Mg ha^{-1} y^{-1}). Across eastern US ecoprovinces, $\Delta B_{observed}$ was positively correlated with $\Delta B_{productivity\ trend}$ and ΔB_{age} but was not significantly correlated with $\Delta B_{disturbance}$ (*SI Appendix*, Fig. S7).

2. Discussion

2.1. Key Findings. Our results show that over the last two decades, forest productivity has tended to increase in regions that have experienced increased precipitation and mild warming (much of the eastern United States), whereas forest productivity has tended to decrease in regions that have experienced decreased precipitation and more severe warming (much of the western United States). These productivity trends are inferred from analyses that control for either stand age or live biomass stock (depending on the model form) as well as biomass losses from mortality and harvest. Thus, the productivity trends we report likely reflect trends in individual tree growth rates, rather than changes in biomass growing stocks

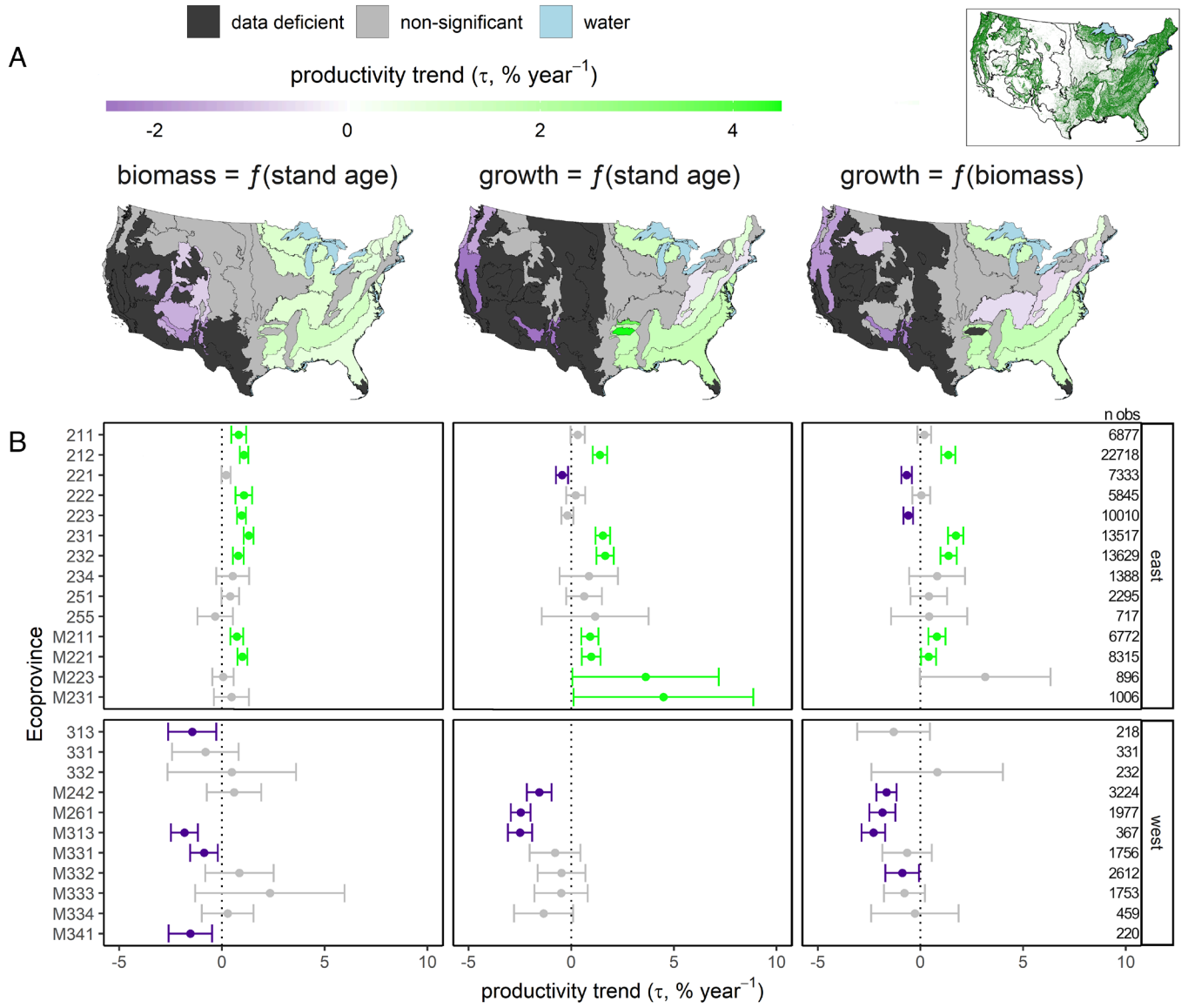

Fig. 1. Productivity trends (~1999 to 2020) for US forests by ecoprovince, estimated from three model forms: biomass = *f*(stand age), growth = *f*(stand age), and growth = *f*(biomass). The *Upper Right Inset* shows forest cover across the coterminous United States. (*A*) Productivity trends (τ) mapped by ecoprovince. Ecoprovinces with τ estimates not significantly different from zero ($P > 0.05$) are colored light gray. Ecoprovinces where no τ estimate is available (due to model non-convergence; see *Materials and Methods* Section 3.4.5.) are colored dark gray. (*B*) τ estimates and 95% CIs by ecoprovince (see map of ecoprovince codes in *SI Appendix*, Fig. S1). Significantly negative τ estimates are colored purple, whereas significantly positive estimates are green. See *SI Appendix*, Tables S2–S4 for details of model fits.

due to disturbance or regrowth. While observed and projected future increases in tree mortality highlight the vulnerability of US forests to climate change (12, 31, 45, 46), our results also demonstrate the potential for non-lethal effects of climate change to weaken or reverse forest carbon sinks.

The significantly positive productivity trends reported here for the eastern United States (Fig. 1 and *SI Appendix*, Fig. S3) contrast with the non-significant trends estimated from an older dataset (38) but are consistent with a more recent study that inferred a significant CO_2 response for eastern US forests (39). Contrasting results from the newer and older studies could potentially reflect methodological differences combined with a small signal-to-noise ratio—i.e., the subtle growth enhancement expected from a ~0.5% y^{-1} increase in atmospheric CO_2 (the mean trend since 1960) relative to the much stronger stand-level effects of disturbance–recovery dynamics. Finding such small signals is critical, because constant (i.e., stationary) disturbance–recovery processes do not affect ecosystem carbon balance over broad spatial or temporal scales (47), whereas even small shifts in mean carbon fluxes (due to CO_2 fertilization or other effects of similar magnitude) can have globally significant cumulative effects (48). The robustness of our results to alternative model forms and data subsets (see below) suggests that the productivity trends reported here reflect real changes in the dynamics of US forests. However, important questions remain, including the mechanisms leading to variation in productivity trends within the eastern United States, some of which are significantly negative (Fig. 1). Some of this variation may be related to the degree of climate warming (Fig. 2 *F* and *I*), effects of invasive insects and pathogens (49), and interactions between climate change and insects or disease (11, 12).

The productivity trends reported here for non-plantation forests are qualitatively similar to ecosystem carbon stock changes reported by the US Forest Service for plantation and non-plantation forests combined (positive in all eastern US states, but of varying sign in

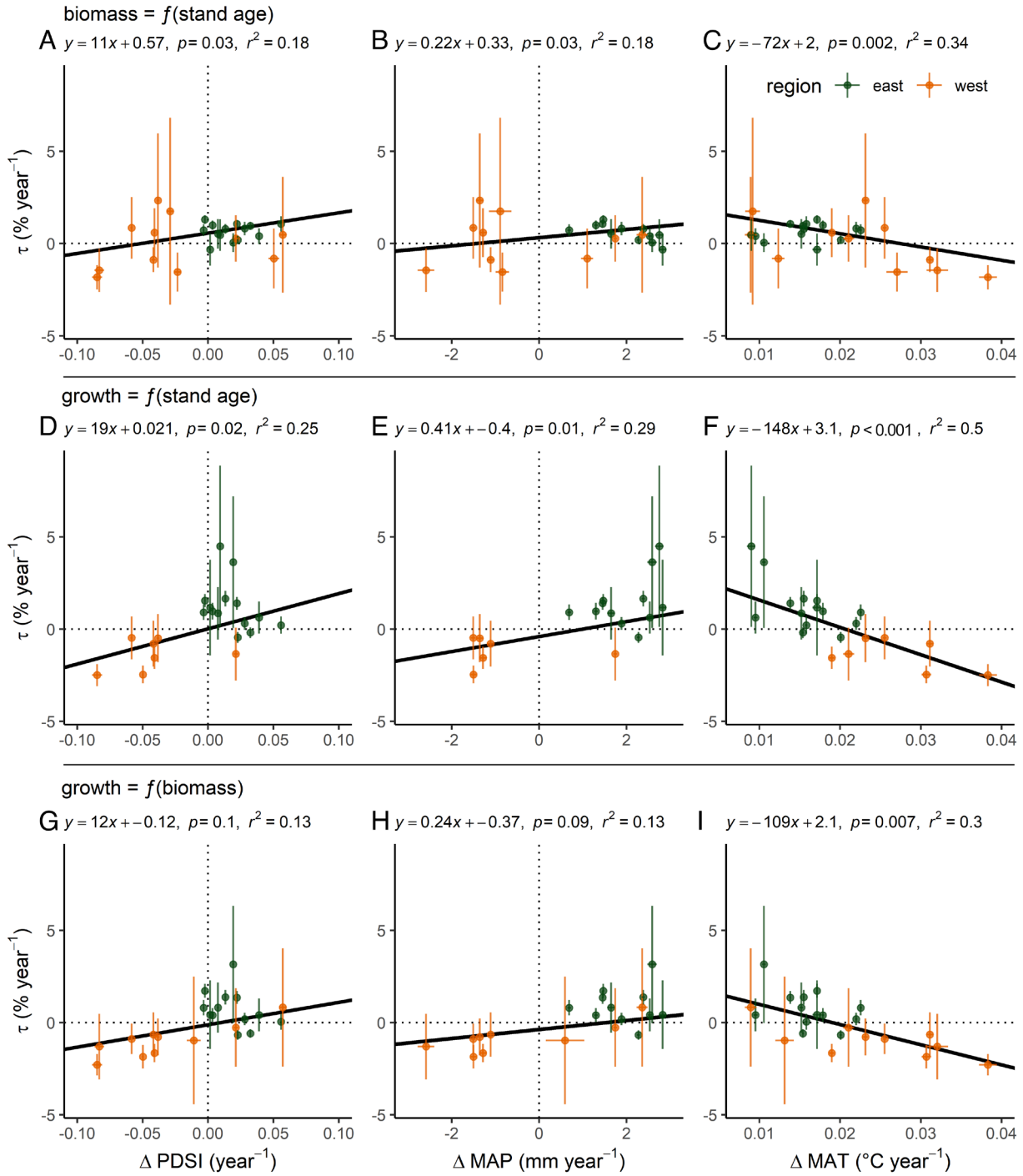

Fig. 2. Relations between productivity trends (τ) and changes in the Palmer Drought Severity Index (ΔPDSI; positive values indicate increases in water balance), mean annual precipitation (ΔMAP), and mean annual temperature (ΔMAT) for US ecoprovinces. Results were qualitatively consistent across the three model forms: (*A*–*C*) biomass = *f*(stand age), (*D*–*F*) growth = *f*(stand age), and (*G*–*I*) growth = *f*(biomass). Productivity trends tend to be positive in ecoprovinces where moisture has increased and warming has been mild and negative in ecoprovinces where moisture has decreased and warming has been more severe (*SI Appendix*, Fig. S5). Error bars are 95% CIs. Thick black lines show linear relations between productivity trends (τ) and climate-change variables; linear model equations, *P*-values for the slopes, and model coefficients of determination are shown at the *Top* of each panel.

western US states), with changes in aboveground biomass stocks accounting for ~70% of total ecosystem carbon stock changes in US forests since 1990 (40). Thus, although our analysis is restricted to aboveground biomass, our findings have important implications for ecosystem carbon balance. In the eastern United States, where data availability permitted decomposing biomass change into different components, forest maturation and increasing productivity contributed, on average, roughly equally to biomass change (Fig. 3*A*), with both components explaining significant variation in biomass change across ecoprovinces (*SI Appendix*, Fig. S7). These findings are qualitatively consistent with reconstructions from ecosystem process models, which indicate important contributions of both age-dependent and environmental factors to global and eastern US carbon sinks (50). In the western United States, negative productivity trends (Fig. 1 and *SI Appendix*, Fig. S3) likely contribute to declining ecosystem carbon stocks in some western

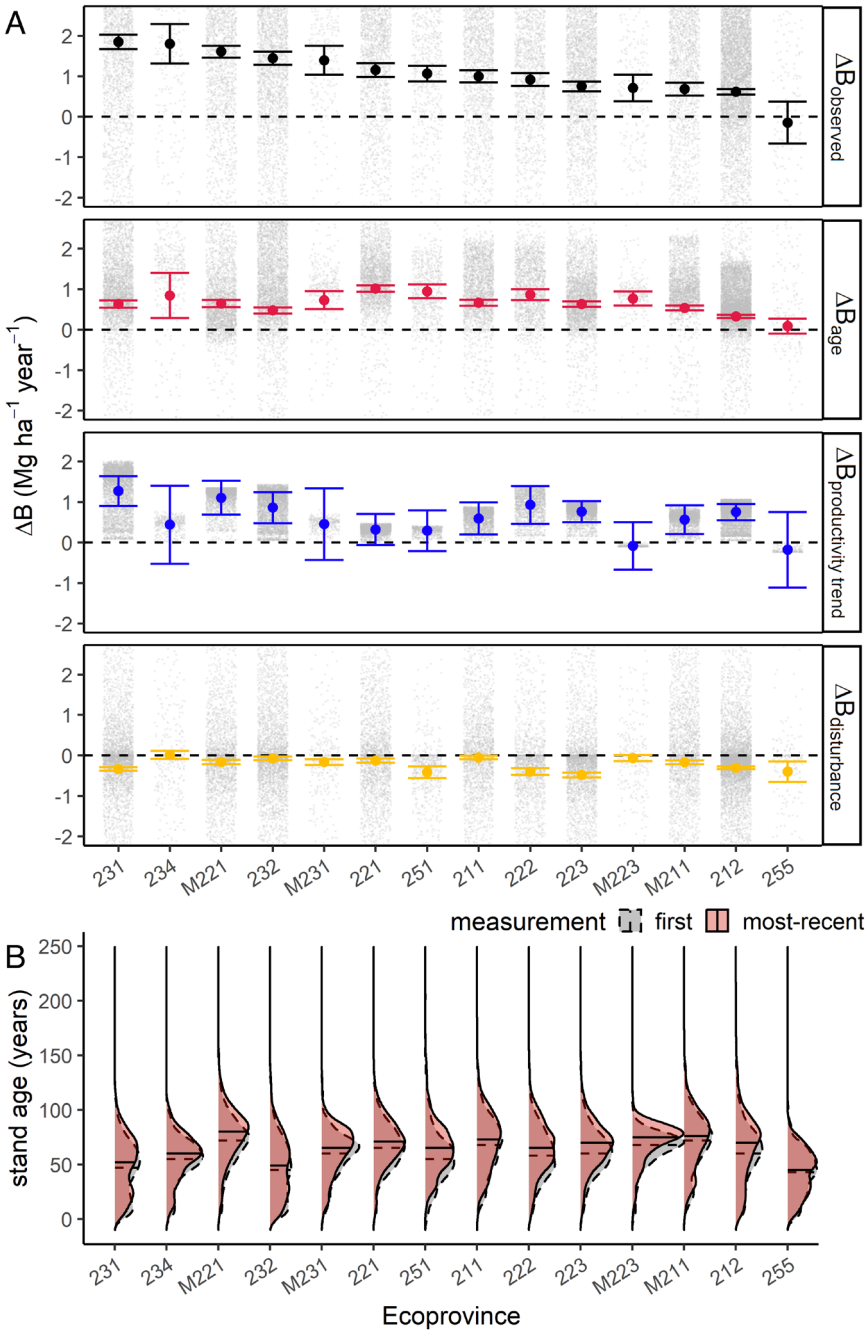

Fig. 3. Components of forest biomass change in the eastern United States. (*A*) Partitioning observed change in aboveground forest biomass ($\Delta B_{observed}$) into stand age (ΔB_{age}), productivity trend ($\Delta B_{productivity\ trend}$), and disturbance ($\Delta B_{disturbance}$) components for 14 eastern US ecoprovinces shows that increases in eastern US forest biomass are driven by both productivity increases (mean $\Delta B_{productivity\ trend}$ across ecoprovinces: 0.65 Mg ha^{-1} y^{-1}) and forest maturation (mean ΔB_{age} across ecoprovinces: 0.58 Mg ha^{-1} y^{-1}). Ecoprovinces are arranged from greatest to least $\Delta B_{observed}$. Gray points show the observed and partitioned biomass change for each FIA plot location from the first to the most recent plot remeasurement, truncated to ΔB of ±2 Mg ha^{-1} y^{-1} (values beyond this range are not shown but were included in the analysis). Bold points and error bars show ecoprovince means and 95% CIs. (*B*) Stand age distributions for the first and most recent remeasurement of each inventory plot. Results in this figure are based on a temporally balanced sample of forest inventory plots (two remeasurements per plot; *SI Appendix*, Fig. S4 and Table S5).

states (40). The sensitivity of productivity trends in US forests to climate change (particularly warming; Fig. 2) mirrors observed and projected changes in tropical forests, where heat and water stress have weakened—and could potentially reverse—biomass carbon sinks (7).

2.2. Robustness of Results. The productivity trends we estimated were mostly consistent across different model forms and different data subsets used to evaluate the potential effects of harvest and unbalanced sampling (*SI Appendix*, Fig. S4 and Table S1). Two of the three model forms we considered (*SI Appendix*, Fig. S2) use stand age—defined in the US forest inventory as the estimated mean age of trees in the dominant size class (44)—which provides ambiguous information in uneven-aged stands and does not always accurately reflect the time since the last major disturbance (51). Nonetheless, we obtained qualitatively similar results from an age-independent model of biomass production as a function of biomass stock, which suggests that our main results are robust to uncertainties or biases associated with stand age. All model forms we considered account for biomass losses due to mortality

and harvest during plot remeasurement intervals. Trends in losses vary among ecoprovinces (*SI Appendix*, Table S5), but these trends account for little of the variation in biomass stock changes (*SI Appendix*, Fig. S7*C*). Estimated productivity trends could, in principle, be confounded with trends in loss rates if our models fail to adequately capture the effects of losses. However, excluding harvested plots did not qualitatively change our results (*SI Appendix*, Fig. S4 and Table S1), which suggests that our analysis captures the effects of changing loss rates and that the productivity trends we report are robust.

2.3. Drivers of Productivity Trends in US Forests. The positive productivity trends we report in eastern US forests are likely due to multiple drivers. There is broad empirical and theoretical support for CO_2 fertilization of forest productivity (13–15), although the strength of the effect is uncertain and likely sensitive to environmental conditions (16, 22, 23, 52). The strongest CO_2 response predicted by theory, a proportional increase in productivity with atmospheric CO_2 (16), is ~0.5% y^{-1} since 1960 or ~0.6% y^{-1} since 2000. A recent study of eastern US forests inferred a ~0.3% y^{-1} increase in wood volume due to CO_2 fertilization from 1970 to 2015 (39), which is well within the theoretical range. In contrast, some trends we report are significantly greater than the theoretical upper bound (Fig. 1 and *SI Appendix*, Tables S2–S5), suggesting a role for additional mechanisms, such as increases in growing season length (53), increases in water balance (54), and nitrogen deposition (9). An analysis of eastern US forests from the 1980s to 2000s showed that changes in biomass were not consistently related to changes in growing season length but were positively correlated with changes in water balance (PDSI) (54). In contrast, our results provide no evidence since ~2000 for increasing productivity trends across eastern US ecoprovinces with increasing PDSI or precipitation (Fig. 2). However, two of the three model forms we considered indicate higher productivity trends in eastern US ecoprovinces that experienced the least warming (Fig. 2). Nitrogen-deposition effects on eastern US forests have been inferred to be as strong or stronger than CO_2 fertilization effects (10), although some studies have reported much weaker effects of nitrogen deposition (9). Factorial experiments with a process-based ecosystem model suggested weak climate effects but strong CO_2 and nitrogen-deposition effects in the mid-Atlantic region of the eastern United States during the 20th century (55). In summary, CO_2 fertilization seems a plausible mechanism contributing to productivity increases in eastern US forests, but other drivers likely contribute as well. Evidence for a direct effect of climate change on eastern US forest productivity trends is weak, although trends within the eastern United States and across the entire coterminous United States suggest that the effects of positive drivers are strongest where warming is mild (Fig. 2).

Negative productivity trends were found for some western US ecoprovinces, where effects of intensifying drought and climate change on tree growth rates are well documented (28, 35, 56, 57). Our results suggest that in the western United States, the effects of these negative drivers on tree growth rates outweigh the effects of CO_2 fertilization or other positive drivers. This finding adds to a growing body of evidence from US forests showing the importance of negative drivers on tree growth. (56, 57). Thus, as ecosystems warm, heat and drought-related plant stress may lead to less realized biomass productivity (58), potentially shifting the dominant driver of productivity trends from CO_2 to vapor pressure deficit (VPD) (59, 60). Increasing temperature and drought stress negatively affect tree carbon balance due to increased metabolic rates (60, 61) and due to the opportunity cost of stomatal closure, which limits the potential for CO_2-stimulated increases of photosynthesis (17, 18). Thus, warming and drought is in effect a twofold stressor on plant function, with increased tree carbon costs affecting both carbon source-sink dynamics within trees and whole-tree growth rates (52). In summary, climate change–induced tree stress appears stronger than the combined effects of any positive drivers in many forests of the western United States. This finding is consistent with regional differences in growth trends in Europe, where climate change–driven tree growth declines in southwestern Europe contrast with growth increases in northern Europe where climate change has been relatively mild (62). Thus, tree growth declines due to increased climate stress may be characteristic of global change responses of precipitation-limited forests across the globe.

2.4. Implications of Our Results for the Terrestrial Carbon Balance. Our results suggest that global terrestrial ecosystem models, including the land components of ESMs, are overly optimistic in their projections of land carbon balance, potentially because climate constraints on terrestrial biomass productivity are not adequately represented. Ecosystem model reconstructions for 2000 to 2019 (63) and ESM projections for the 21st century (64) indicate stronger carbon sinks in the eastern compared to western United States but fail to capture the negative carbon balances observed in much of the western United States (40). In addition to intensifying mortality and fire regimes—e.g., the large increase in carbon emissions from US fires from the late 1990s to the early 2000s (40)—our results suggest that productivity declines have contributed to ecosystem carbon losses since ~1999 in the western United States. Conversely, our results demonstrate how productivity increases are likely maximized in ecosystems that are energy- rather than water-limited, and where drought and heat stress are mild (8, 22, 65). At the global scale, ESMs predict that the positive response of terrestrial carbon storage to CO_2 fertilization is stronger than the negative response to climate change (4). However, our results suggest that the climate response has already overwhelmed the CO_2 response in much of the United States, and that the future global balance of these opposing forces may depend on the geographic extent of drought and heat stress.

3. Materials and Methods

3.1. US National Forest Inventory Data. The Forest Inventory and Analysis (FIA) program of the US Department of Agriculture Forest Service monitors permanent sample plots that are systematically distributed across all public and private forest land in the United States. Starting in the late-1990s, FIA began implementing a national standardized annual inventory (36), with 1 plot per ~2,428 ha; ~10% of western US plots and ~20% of eastern US plots are remeasured each year (remeasurement intervals of ~10 and ~5 y, respectively). Due to complications arising from changes in plot designs and the non-public plot identifiers required to link plot locations across current and older designs, we restricted our analysis to plot measurements collected using the current annual design (FIA 2.0). Our analysis is based on FIA database version 9.0.1 (66). The FIA dataset is an unbiased sample of US forests but has several limitations. These limitations limit the temporal resolution of our analysis and our power to detect productivity trends but should not bias our results (see Section 3.8. for details).

Under the annual design, trees with a diameter ≥12.7 cm (typically measured at 1.37 m height) are measured within four circular subplots (7.3 m radius; plot sample area of 0.067 ha), and trees with a diameter between 2.54 and 12.7 cm are measured within 2.1-m radius microplots (one per subplot). In some western US states, the subplot radius is optionally expanded to 18.2 m to sample large trees (e.g., diameter >53 cm). The status of each tree (live, dead, or cut) is reported at the time of each plot measurement (66). FIA reports the aboveground biomass of trees with diameter 2.54 to 12.7 cm based on national-scale allometries (67) and of larger trees based on more detailed methodology that incorporates

regional variation in allometry and field-based estimates of sound wood volume (not rotten or missing) for individual trees (68).

Plot-level information reported by FIA includes the approximate latitude-longitude; ecological subsection codes that identify areas of similar geology, soil, and climate [we aggregated these codes to the ecoprovince level (43)]; and the measurement dates, which we converted to decimal years as (measurement year) + (measurement month)/12. Each FIA plot has one or more mapped conditions, which describe forest characteristics such as structure, composition, disturbance, and ownership (44). FIA reports stand age for each condition, which is defined as the mean age of trees in the dominant size class (44). Stand age is initially estimated by coring two or three overstory trees and is then incremented over time if no serious disturbance has occurred, or re-estimated as needed (44). We used stand age in our analyses as a biomass-independent measure of stand development (50, 69).

3.2. Plot Selection Criteria. We limited our analyses to plots that were measured at least twice under the current annual design. To avoid complications due to within-plot heterogeneity in disturbance history or environmental conditions, we restricted our analyses to plots that were dominated by a single condition at every measurement time ("condition proportion unadjusted" in the FIA Condition table ≥ 0.95), and we applied descriptors of the dominant condition (e.g., stand age) to the entire plot. Based on these condition attributes, we further restricted our analysis to plots classified as accessible forest land (current or previous canopy cover of at least 10% in an area of at least 0.4 ha and at least 36.6 m wide), plots that lacked clear evidence of artificial regeneration (i.e., we excluded tree plantations), and plots with an inherent capacity for wood volume growth of at least 1.4 $m^3\ ha^{-1}\ y^{-1}$ (which excludes plots assigned to the lowest of FIA's seven site productivity classes). Finally, plots with outlying biomass growth estimates were excluded (0.2% of plots; see details in Section 3.3. below).

Unless stated otherwise, all our analyses used the same set of plot records, which included all plot remeasurements that met our selection criteria described above. For example, if a plot location was measured three times, then it contributed two observations to our analyses, with response variables in our models (biomass stock and biomass growth; see details below) recorded at times 2 and 3 (in this example, growth would be calculated over the intervals between times 1 to 2 and times 2 to 3). After applying all filters, the dataset used for our main analyses had measurement years (at the time of each remeasurement) ranging from 1998 to 2021. We report our study period as ~1999 to 2020, with these years representing the first and 99th percentiles of the remeasurement dates.

3.3. Estimating Aboveground Biomass Stocks and Growth. We calculated the live aboveground biomass stock (B_t; Mg ha^{-1}) for each plot at each measurement (time t) by summing the product of individual tree aboveground biomass (AGB) estimates (aboveground wood dry mass values reported by FIA) and their expansion factors (TPHa: the number of trees per hectare that a tallied tree represents, which is the inverse of the area on which it is sampled) for all trees ($i = 1$ to n) alive at time t: $B_t = \sum_{i=1}^{n} \left(\mathrm{AGB}_i \times \mathrm{TPHa}_i\right)$. The TPHa values used here are a constant (2.47 acres per hectare) times the "trees per acre unadjusted" values reported in the FIA Tree table.

We used two methods to estimate plot-level biomass growth rates (G, Mg $ha^{-1}\ y^{-1}$) over a plot remeasurement interval (from t to $t + \Delta t$). The two methods are described below and are analogous to the two "stand increment" approaches illustrated in Fig. 2 of Clark et al. (70). For many FIA plots, these two approaches yield different estimates of G, due to changes over time in the expansion factors for individual trees. For example, a tree's TPHa value decreases when its diameter crosses the 12.7 cm threshold due to the difference in sampling area between microplots and subplots, which can result in negative G estimates when employing the first method described below. Cases where the two methods yield very different results may indicate database errors or situations where one or both methods have high variance.

The first method, which we refer to as the "mass balance" method (and which was used for all analyses of G that we report in this paper), uses the full sample of trees at times t and $t + \Delta t$. The change in biomass stocks is $B_{t+\Delta t} - B_t = \Delta t \cdot G - M_t - C_t$, where B_t is defined as above, and M_t and C_t, respectively, are the time-t biomass stocks of trees that died or were cut (harvested) between times t and $t + \Delta t$ (71). Rearranging the above equation yields the mass balance estimate of the biomass growth rate between time t and $t + \Delta t$: $G = (B_{t+\Delta t} - B_t + M_t + C_t) / \Delta t$. This method is based only on biomass stocks, and the relevant expansion factors (trees per acre unadjusted) are reported in the FIA Tree table at times t and $t + \Delta t$ for all tallied trees.

The second method, which we refer to as the "increment sum" method, sums the annualized biomass increments of individual trees from time t to $t + \Delta t$ and weights each tree by its time-t growth expansion factor (38, 72). A complication with implementing this method with the data provided in the FIA Tree table is that growth expansion factors ("growth trees per acre unadjusted") are only reported for trees with diameter ≥12.7 cm. An additional complication involves "ingrowth trees" in microplots, which enter the tallied diameter class between times t and $t + \Delta t$ and thus have no reported expansion factor at time t. In contrast, the mass balance method automatically accounts for ingrowth (71). Because our aim was to use the increment sum method only as a rough check on the mass balance method, we implemented the increment sum method using the FIA Tree table as follows: We used biomass stock (rather than growth) expansion factors (because these are reported for all trees with diameter ≥2.54 cm), and we assigned the standard microplot expansion factor (assuming four microplots per plot) to ingrowth trees, which we assumed had AGB of 0 at time t. This implementation should result in only small errors in most cases, and thus can serve as a rough consistency check for the mass balance method.

To reduce noise in our main analyses, we excluded two types of outliers from the G estimates (mass balance method). We excluded the extreme lower and upper 0.05% tails (0.1% combined) of the distribution of G across all plot remeasurements, and we excluded the extreme lower and upper 0.05% tails (0.1% combined) of the distribution of differences between the mass balance and increment sum estimates of G. For consistency, plot records that were excluded from our analyses of G were also excluded from other analyses in our study. Excluding these outliers improved model fits in some ecoprovinces but did not qualitatively affect our main results or conclusions.

3.4. Fitting Biomass and Growth Models to Quantify Productivity Trends.

3.4.1. Overview of model forms. For each ecoprovince, we fit non-linear regression models to quantify "productivity trends" (τ; % y^{-1}) associated with temporal trends in biomass stocks (B) or growth (G) (*SI Appendix*, Figs. S2, S8, and S9). All models share the same general form:

$$y = f_d(\text{disturbance}) \times f_y(\text{year}) \times f(x), \qquad [1]$$

where the response variable (y, either biomass stock or biomass growth) is the product of three functions (each with fitted parameters) representing the effects of disturbance (biomass losses during a remeasurement interval due to mortality or harvest), year (measurement date), and x (either stand age or biomass stock). Because the disturbance and year functions were used in all models, we label the models according to y and $f(x)$ as follows: biomass = f(stand age), growth = f(stand age), and growth = f(biomass) (*SI Appendix*, Fig. S2). For consistency, and as explained in Section 3.2., both response variables (B and G) were recorded at the end of a given remeasurement interval (time $t + \Delta t$). For all model forms, biomass loss (for the disturbance function) was measured over the interval from t to $t + \Delta t$. For the biomass = f(stand age) models, stand age was recorded at time $t + \Delta t$, as this age is most relevant to modeling biomass at time $t + \Delta t$; for simplicity, we also recorded year (measurement date) for the biomass = f(stand age) models at time $t + \Delta t$ (although we recognize that in reality, biomass stock reflects growing conditions over the entire history of a stand). In contrast, for the growth models, stand age was recorded at time t (to capture the effects of antecedent conditions on growth), and year was recorded at the midpoint between t and $t + \Delta t$ (i.e., the mean year during the growth interval).

3.4.2. f(x)—the age or biomass function. We explored two functional forms for $f(x)$ in Eq. **1**, which are illustrated in *SI Appendix*, Fig. S2. One set of forms is based on the Michaelis–Menten function (sometimes called the Monod function), which has previously been shown to provide a good fit to biomass vs. age relationships in US forests (73). We modified the standard two-parameter Michaelis–Menten function by including y-intercept and shape parameters (e.g., to allow for sigmoid curves):

$$f(x) = pA + \frac{(1-p)\ A \cdot x^s}{\left(k^s + x^s\right)}, \qquad [2]$$

where A is the asymptote, k is the half-saturation constant, pA is the y-intercept, and s is the shape parameter. If $p = 0$ and $s = 1$, then Eq. **2** reduces to the standard two-parameter form: $f(x) = Ax / (k + x)$. The second form is based on the log-normal growth function of Uriarte et al. (74), modified here to include a y-intercept:

$$f(x) = a + b \cdot e^{-\left(\frac{\ln(x/c)}{d}\right)^2}, \quad [3]$$

where a is both the y-intercept and the limiting (large-x) value of y, $a + b$ is the peak height of the curve, c is the x-value at the peak, and d is a shape parameter. Based on preliminary analyses, we considered Eqs. **2** and **3** for biomass = f(age), only Eq. **3** for growth = f(age), and only Eq. **2** for growth = f(biomass). For Eq. **2**, we considered the two-parameter Michaelis–Menten version, three-parameter versions (with p or s alone), and the four-parameter version (with p and s). In cases where multiple functional forms were considered (e.g., different Michaelis–Menten versions), we report results for the form with the lowest AIC (see model-fitting details below).

3.4.3. f_d(disturbance)—the effect of biomass loss (α). The disturbance term in Eq. **1** accounts for the effects of biomass losses during a remeasurement interval due to morality or harvest, assuming that biomass stocks or growth are reduced in proportion to the fraction of biomass lost: $f_d(\text{disturbance}) = 1 - \alpha L$, where α is a fitted parameter, and L is the fraction of biomass lost to mortality or harvest between times t and $t + \Delta t$; i.e., $L = (M_t + C_t) / B_t$. The fitted value of α can represent a range of disturbance responses, including (but not limited to) complete compensation for biomass losses ($\alpha = 0$), no compensation ($\alpha = 1$), or over-compensation ($\alpha < 0$). Each ecoprovince model was fit with and without the f_d(disturbance) term, and we report results for the version with the lower AIC (see model-fitting details below). The f_d(disturbance) term (and thus the α parameter) was included in nearly all cases (*SI Appendix*, Tables S2–S5).

3.4.4. f_y(year)—the effect of productivity trends (τ). The year term in Eq. **1** represents trends in biomass stocks or growth (which we collectively refer to as productivity trends) that cannot be explained by other model terms: $f_y(\text{year}) = 1 + (\tau / 100)(\text{year} - 1990)$ where τ (% y^{-1}) is the productivity trend, year is the measurement date (expressed as year + month/12), and 1990 is a reference year chosen to predate the earliest plot remeasurement in our dataset. The f_y(year) function can be interpreted as a multiplier that causes a linear trend over time in the height of the $f(x)$ curve, with positive or negative τ, respectively, leading to upward or downward trends in $f(x)$ (*SI Appendix*, Fig. S2). All models we report include the f_y(year) term (model selection was not applied to this term).

3.4.5. Model fitting. Models were fit separately for each ecoprovince using the "*nls*" function (75) in R (v4.2.0) (76). Observations were weighted in *nls* in proportion to their inverse variance, with the weights determined as follows: First, we fit unweighted models in *nls*. Second, we separated the observations into x-bins of equal sample-size (typically 20 bins, but 10 bins in ecoprovinces with insufficient data for 20 bins). Third, we calculated within each bin the mean of y, the SD of the residuals (from the unweighted *nls* model), and the variance of the residuals. For the biomass = f(age) and growth = f(age) analyses, the mean was roughly proportional to the residual SD in most ecoprovinces, indicating that the mean squared (y^2) was roughly proportional to the residual variance. Therefore, for these two model forms, we implemented inverse-variance weighting of observations by assigning weights in bin i as $1 / \overline{y}_i^{\,2}$. In contrast, for the growth = f(biomass) analysis, the mean was roughly proportional to the residual variance in most ecoprovinces. Therefore, for this model form, we implemented inverse-variance weighting of observations by assigning weights in bin i as $1 / y_i$. Each model was fit to data from all bins simultaneously; thus, bins were only used to assign weights and to visualize model predictions (*SI Appendix*, Figs. S8 and S9). We first attempted to fit models using the default Gauss–Newton optimization method in *nls*; in cases where models failed to converge with the Gauss–Newton method, we then used the "nl2sol" algorithm in *nls*, constraining model parameters to realistic ranges. Models were considered data-deficient (no results reported) if the model failed to converge (with both *nls* methods described above), if the model repeatedly converged on implausible parameter estimates from different initial conditions, or if the estimated 95% CI for τ was wider than 10% y^{-1} (which we interpreted as a lack of useful information). We refer to these cases as "data-deficient" because they were never observed in ecoprovinces with $n > 2{,}000$ plot remeasurements. For conciseness in the Fig. 1 caption, we use the phrase "model non-convergence" to refer to the broader set of data-deficient criteria described here. In some ecoprovinces with $n < 2{,}000$, models converged with plausible and well-constrained parameter values for some model forms but not others (Fig. 1). Thus, convergence is not a simple function of sample size and likely depends on the signal-to-noise ratio, which may differ substantially among the three model forms in each ecoprovince.

3.4.6. Alternative forms of analysis and data subsets. To evaluate the robustness of the model results, we considered several alternative forms of analysis and data subsets. Fitting models in *nls* using unweighted observations led to similar results as the inverse-variance weighting described above. We also considered two approaches for implementing plot-level random effects to account for covariance across multiple remeasurements at a given plot location (on average 2.3 remeasurements, or 3.3 measurements, per plot in the East; and 1.1 remeasurements, or 2.1 measurements, in the West). These methods included the nonlinear mixed effects "*nlme*" function in R (77) and a hierarchical Bayesian approach in JAGS (78). However, both the nonlinear mixed effects models and plot-level random effect parameters in the Bayesian models failed to converge, likely due to the small, yet variable, number of remeasurements and weak plot-level covariance of model residuals, suggesting that plot-level random effects were not necessary.

To evaluate effects of the unbalanced design (different numbers of remeasurements at different plot locations), we analyzed a "temporally-balanced" dataset (*SI Appendix*, Fig. S4) that included two remeasurements per plot location, with the first remeasurement date typically prior to 2010, and the second one typically after 2010. Plots that were only remeasured once were excluded from this analysis. For plots with multiple remeasurements, we used only the first and last remeasurements in this analysis, so that each plot was represented twice. To evaluate the robustness of our results to harvest effects, we analyzed an "excluding timber harvest" dataset (*SI Appendix*, Fig. S4), in which we began with the full dataset used in our main analyses, and then excluded plot locations where any tree harvest was reported during any remeasurement interval.

3.5. Regional Productivity Trends: Weighted-Mean τ Estimates. To quantify regional productivity trends, we calculated weighted averages of the ecoprovince-scale productivity trends (τ; *SI Appendix*, Tables S2–S4) for the eastern and western United States (*SI Appendix*, Fig. S3). We used inverse-variance weighted averaging because this method provides an unbiased and minimum-variance estimate of the regional mean (79). The variance of each τ estimate is the square of its SE. We estimated the width of the 95% CI for each regional mean as $\pm 1.96 \times \sigma_{\text{regional}}$, where $\sigma^2_{\text{regional}} = 1/\left(\sum_i 1/\sigma_i^2\right)$, and σ_i^2 is the variance of the τ estimate in ecoprovince i (79).

3.6. Relating Productivity Trends to Changes in Climate. We quantified the trend in the mean annual Palmer Drought Severity Index (PDSI) (80), mean annual precipitation (MAP), and mean annual temperature (MAT) from 1972 to 2022 for each FIA plot location based on the approximate plot locations reported in the public FIA database. These plot-level trends were then averaged within each ecoprovince (Table 1). Precipitation and temperature data (4-km spatial resolution) were obtained from PRISM (81), and PDSI data (4-km spatial resolution) were obtained from West Wide Drought Tracker (82). The mean rate of change for PDSI, MAP, and MAT (ΔPDSI: unitless y^{-1}, ΔMAP: mm y^{-1}, and ΔMAT: °C y^{-1}, respectively) over the 50-y interval (1972 to 2022) for each FIA plot location was estimated from ordinary least squares regressions of each climate variable vs. year. To evaluate relationships between productivity trends (τ) and climate change variables, we first averaged ΔPDSI, ΔMAP, and ΔMAT across all plot locations within each ecoprovince, and we then regressed τ vs. each climate change variable. In these regressions, each τ estimate was weighted by the inverse of its variance (the square of the SE of the τ estimate).

3.7. Partitioning Changes in Biomass Stocks. We used the biomass = f(age) model to partition the annualized change in aboveground biomass stocks (ΔB, Mg ha^{-1} y^{-1}) into three components: change in B due to change in biomass losses ($\Delta B_{\text{disturbance}}$), change in B due to productivity trends ($\Delta B_{\text{productivity trend}}$), and change in B due to change in the stand age distribution (ΔB_{age}). These three components correspond, respectively, to the three components of Eq. **1**, which, for the biomass = f(age) model, has the following form:

$$B = f_d(\text{disturbance}) \times f_y(\text{year}) \times f(\text{age}). \quad [4]$$

Because the $f_d(\text{disturbance})$ function requires fractional losses (L) calculated over a remeasurement interval, quantifying change in $f_d(\text{disturbance})$ requires three or more measurements (two or more remeasurements). Therefore, we restricted this analysis to the eastern United States, where two or more remeasurements were available for a large sample of plots, and we used the temporally balanced dataset (two remeasurements per plot location; *SI Appendix*, Fig. S4) to minimize sampling effects. The parameter estimates used to partition ΔB (Eq. **4** fit to the temporally balanced dataset for eastern US ecoprovinces) are reported in *SI Appendix*, Table S5.

We estimated the observed annualized change in B ($\Delta B_{observed}$; $Mg{\cdot}ha^{-1}{\cdot}y^{-1}$) as follows: We use "T" to denote a plot remeasurement date (previously denoted as "$t + \Delta t$"), and we use the subscripts "first" and "last" to denote the first and last remeasurements, respectively (i.e., the two remeasurements of each plot in the temporally-balanced dataset). For a given plot, we calculated $\Delta B_{observed} = (B_{last} - B_{first})/(T_{last} - T_{first})$, where B_{last} and B_{first} are the observed biomass stocks at times T_{last} and T_{first}. For each ecoprovince, we report the across-plot mean of these $\Delta B_{observed}$ values, and we estimate 95% CIs as ± 1.96 times the SEM (Fig. 3 and *SI Appendix*, Figs. S6 and S7).

Our general approach to partitioning ΔB is to quantify the effect of each of the three terms in Eq. **4** (using the parameter estimates in *SI Appendix*, Table S5) while holding the other two terms constant. Methods for estimating the ecoprovince mean ΔB components and their uncertainties are explained in *SI Appendix*, *Supplementary Information Text*.

3.8. Limitations of FIA Data and Potential Biases. FIA provides an unbiased sample of US forests on both public and private land (36) but has several limitations relevant to our study. First, although there is a large sample of plots, each plot is relatively small, so that the plot-level data have high variance (noise). The combination of noise and the limited sample size in some ecoprovinces likely results in limited power to detect productivity trends. Thus, the non-significant (or non-convergent) trends we report for some ecoprovinces do not provide strong evidence for constant productivity over time. Second, the roughly 5- to 10-y plot remeasurement intervals preclude direct quantification of interannual variability in carbon stocks and fluxes, which can be substantial (6); therefore, our analysis focuses on mean trends over ~1999 to 2020. Third, the limited temporal resolution of remeasurements leads to underestimating rates of biomass production (growth) because no direct measurements are available to quantify the growth of individual trees that die or are harvested during remeasurement intervals. While it is possible to estimate this unobserved growth component using models, we restricted our analysis to growth that can be quantified directly from the inventory data. This omission results in growth estimates that are too low whenever mortality or harvest occur. However, this form of bias should not qualitatively affect our estimated productivity trends, because our models account for mortality and harvest losses. Consistent with this expectation, our productivity trend estimates were similar for data subsets that included or excluded harvested plots (*SI Appendix*, Fig. S4 and Table S1); i.e., harvest losses, which would lead to greater underestimates of growth than natural mortality alone, had little impact on our estimated productivity trends. Finally, FIA reports biomass values that are estimated from allometries. Uncertainty or bias in the allometries would lead to errors in the plot-level biomass stock and growth values that we analyzed but are unlikely to systematically bias our main results.

Data, Materials, and Software Availability. All data used in this manuscript are publicly available through the USDA Forest Service Forest Inventory and Analysis program (83), the PRISM Climate Group (81), and the West Wide Drought Tracker (82, 84). All analyses are contained and documented on a GitHub repository (85).

ACKNOWLEDGMENTS. We thank two anonymous reviewers for thoughtful comments that improved our paper. We thankfully acknowledge all USFS FIA personnel including administrators, field crews, data curators, and scientists for the collective development of the FIA database. This work was funded by USDA Forest Service grant 21-JV-11242305-097.

Author affiliations: [a]Department of Biology, University of Florida, Gainesville, FL 32611; [b]Northern Research Station, United States Department of Agriculture Forest Service, Saint Paul, MN 55108; [c]School for Environment and Sustainability, University of Michigan, Ann Arbor, MI 48109; and [d]School of Forest, Fisheries, and Geomatics Sciences, University of Florida, Gainesville, FL 32611

1. C. Le Quéré *et al.*, Trends in the sources and sinks of carbon dioxide. *Nat. Geosci.* **2**, 831–836 (2009).
2. P. Friedlingstein *et al.*, Global carbon budget 2021. *Earth Syst. Sci. Data Discuss.* **14**, 1917–2022 (2021).
3. P. Friedlingstein *et al.*, Uncertainties in CMIP5 climate projections due to carbon cycle feedbacks. *J. Clim.* **27**, 511–526 (2014).
4. V. K. Arora *et al.*, Carbon–concentration and carbon–climate feedbacks in CMIP6 models and their comparison to CMIP5 models. *Biogeosciences* **17**, 4173–4222 (2020).
5. Y. Pan *et al.*, A large and persistent carbon sink in the world's forests. *Science* **333**, 988–993 (2011).
6. L. Xu *et al.*, Changes in global terrestrial live biomass over the 21st century. *Sci. Adv.* **7**, eabe9829 (2021).
7. W. Hubau *et al.*, Asynchronous carbon sink saturation in African and Amazonian tropical forests. *Nature* **579**, 80–87 (2020).
8. N. G. McDowell *et al.*, Pervasive shifts in forest dynamics in a changing world. *Science* **368**, eaaz9463 (2020).
9. D. S. Reay, F. Dentener, P. Smith, J. Grace, R. A. Feely, Global nitrogen deposition and carbon sinks. *Nat. Geosci.* **1**, 430–437 (2008).
10. R. Quinn Thomas, C. D. Canham, K. C. Weathers, C. L. Goodale, Increased tree carbon storage in response to nitrogen deposition in the US. *Nat. Geosci.* **3**, 13–17 (2010).
11. R. Seidl *et al.*, Forest disturbances under climate change. *Nat. Clim. Change* **7**, 395–402 (2017).
12. W. R. L. Anderegg *et al.*, Future climate risks from stress, insects and fire across US forests. *Ecol. Lett.* **25**, 1510–1520 (2022).
13. D. Schimel, B. B. Stephens, J. B. Fisher, Effect of increasing CO_2 on the terrestrial carbon cycle. *Proc. Natl. Acad. Sci. U.S.A.* **112**, 436–441 (2015).
14. V. Haverd *et al.*, Higher than expected CO_2 fertilization inferred from leaf to global observations. *Glob. Change Biol.* **26**, 2390–2402 (2020).
15. C. Chen, W. J. Riley, I. C. Prentice, T. F. Keenan, CO_2 fertilization of terrestrial photosynthesis inferred from site to global scales. *Proc. Natl. Acad. Sci. U.S.A.* **119**, e2115627119 (2022).
16. A. P. Walker *et al.*, Integrating the evidence for a terrestrial carbon sink caused by increasing atmospheric CO_2. *New Phytol.* **229**, 2413–2445 (2021).
17. E. A. Ainsworth, S. P. Long, What have we learned from 15 years of free-air CO_2 enrichment (FACE)? A meta-analytic review of the responses of photosynthesis, canopy properties and plant production to rising CO_2. *New Phytol.* **165**, 351–372 (2005).
18. A. Gardner *et al.*, Optimal stomatal theory predicts CO_2 responses of stomatal conductance in both gymnosperm and angiosperm trees. *New Phytol.* **237**, 1229–1241 (2023).
19. C. Körner *et al.*, Carbon flux and growth in mature deciduous forest trees exposed to elevated CO_2. *Science* **309**, 1360–1362 (2005).
20. P. S. Curtis, C. M. Gough, Forest aging, disturbance and the carbon cycle. *New Phytol.* **219**, 1188–1193 (2018).
21. T. F. Keenan, C. A. Williams, The terrestrial carbon sink. *Annu. Rev. Environ. Resour.* **43**, 219–243 (2018).
22. C. Körner, J. Morgan, R. Norby, "CO_2 fertilization: When, where, how much?" in *Terrestrial Ecosystems in a Changing World*, *Global Change–The IGBP Series*, J. G. Canadell, D. E. Pataki, L. F. Pitelka, Eds. (Springer, 2007), pp. 9–21.
23. F. Li, D. Guo, X. Gao, X. Zhao, Water deficit modulates the CO_2 fertilization effect on plant gas exchange and leaf-level water use efficiency: A meta-analysis. *Front. Plant Sci.* **12**, 775477 (2021).
24. A. P. Walker *et al.*, Decadal biomass increment in early secondary succession woody ecosystems is increased by CO_2 enrichment. *Nat. Commun.* **10**, 454 (2019).
25. R. J. Norby, J. M. Warren, C. M. Iversen, B. E. Medlyn, R. E. McMurtrie, CO_2 enhancement of forest productivity constrained by limited nitrogen availability. *Proc. Natl. Acad. Sci. U.S.A.* **107**, 19368–19373 (2010).
26. C. Terrer *et al.*, Nitrogen and phosphorus constrain the CO_2 fertilization of global plant biomass. *Nat. Clim. Change* **9**, 684–689 (2019).
27. R. Birdsey, K. Pregitzer, A. Lucier, Forest carbon management in the United States. *J. Environ. Qual.* **35**, 1461–1469 (2006).
28. A. P. Williams *et al.*, Forest responses to increasing aridity and warmth in the southwestern United States. *Proc. Natl. Acad. Sci. U.S.A.* **107**, 21289–21294 (2010).
29. C. D. Allen, D. D. Breshears, N. G. McDowell, On underestimation of global vulnerability to tree mortality and forest die-off from hotter drought in the Anthropocene. *Ecosphere* **6**, art129 (2015).
30. W. M. Hammond *et al.*, Global field observations of tree die-off reveal hotter-drought fingerprint for Earth's forests. *Nat. Commun.* **13**, 1761 (2022).
31. P. J. van Mantgem *et al.*, Widespread increase of tree mortality rates in the western United States. *Science* **323**, 521–524 (2009).
32. D. Bauman *et al.*, Tropical tree mortality has increased with rising atmospheric water stress. *Nature* **608**, 528–533 (2022).
33. L. C. R. Silva, M. Anand, Probing for the influence of atmospheric CO_2 and climate change on forest ecosystems across biomes. *Glob. Ecol. Biogeogr.* **22**, 83–92 (2013).
34. R. J. W. Brienen *et al.*, Long-term decline of the Amazon carbon sink. *Nature* **519**, 344–348 (2015).
35. A. Cabon, R. J. DeRose, J. D. Shaw, W. R. L. Anderegg, Declining tree growth resilience mediates subsequent forest mortality in the US Mountain West. *Glob. Change Biol.* **29**, 4826–4841 (2023).
36. W. A. Bechtold, P. L. Patterson, Eds., The enhanced forest inventory and analysis program–national sampling design and estimation procedures. *Gen Tech Rep SRS-80 Asheville NC US Dep. Agric. For. Serv. South. Res. Stn. 85 P* **080** (Department of Agriculture, US, 2005).
37. J. M. Vose *et al.* "Forests" in Impacts, Risks, and Adaptation in the United States: Fourth National Climate Assessment, Volume II., D.R. Reidmiller, C.W. Avery, D.R. Easterling, K.E. Kunkel, K.L.M. Lewis, T.K. Maycock, B.C. Stewart, Eds. (U.S. Global Change Research Program, Washington, DC, USA, 2018) pp. 232–267.
38. J. P. Caspersen *et al.*, Contributions of land-use history to carbon accumulation in U.S. forests. *Science* **290**, 1148–1151 (2000).
39. E. C. Davis, B. Sohngen, D. J. Lewis, The effect of carbon fertilization on naturally regenerated and planted US forests. *Nat. Commun.* **13**, 5490 (2022).

40. G. M. Domke *et al.* "Greenhouse Gas Emissions and Removals From Forest Land, Woodlands, Urban Trees, and Harvested Wood Products in the United States, 1990–2020" (U.S. Department of Agriculture, Forest Service, Northern Research Station, 2023), 10.2737/fs-ru-382.
41. C. L. Goodale *et al.*, Forest carbon sinks in the northern hemisphere. *Ecol. Appl.* **12**, 891–899 (2002).
42. D. Schimel *et al.*, Contribution of increasing CO_2 and climate to carbon storage by ecosystems in the United States. *Science* **287**, 2004–2006 (2000).
43. W. H. McNab *et al.*, "Description of ecological subregions: Sections of the conterminous United States" (U.S. Department of Agriculture, Forest Service, 2007), 10.2737/wo-gtr-76b.
44. United States Department of Agriculture, Forest Service, "Forest Inventory and Analysis National Core Field Guide, Volume I: Field Data Collection Procedures for Phase 2 Plots" (U.S. Department of Agriculture, Forest Service, 2022).
45. N. G. McDowell *et al.*, Multi-scale predictions of massive conifer mortality due to chronic temperature rise. *Nat. Clim. Change* **6**, 295–300 (2016).
46. D. D. Breshears *et al.*, Regional vegetation die-off in response to global-change-type drought. *Proc. Natl. Acad. Sci. U.S.A.* **102**, 15144–15148 (2005).
47. M. E. Harmon, Carbon sequestration in forests: Addressing the scale question. *J. For.* **99**, 24–29 (2001).
48. Y. He *et al.*, CO_2 fertilization contributed more than half of the observed forest biomass increase in northern extra-tropical land. *Glob. Change Biol.* **29**, 4313–4326 (2023).
49. S. Fei, R. S. Morin, C. M. Oswalt, A. M. Liebhold, Biomass losses resulting from insect and disease invasions in US forests. *Proc. Natl. Acad. Sci. U.S.A.* **116**, 17371–17376 (2019).
50. T. A. M. Pugh *et al.*, Role of forest regrowth in global carbon sink dynamics. *Proc. Natl. Acad. Sci. U.S.A.* **116**, 4382–4387 (2019).
51. J. T. Stevens *et al.*, Average stand age from forest inventory plots does not describe historical fire regimes in ponderosa pine and mixed-conifer forests of western North America. *PLoS One* **11**, e0147688 (2016).
52. A. Cabon *et al.*, Cross-biome synthesis of source versus sink limits to tree growth. *Science* **376**, 758–761 (2022).
53. X. Yue, N. Unger, T. F. Keenan, X. Zhang, C. S. Vogel, Probing the past 30-year phenology trend of US deciduous forests. *Biogeosciences* **12**, 4693–4709 (2015).
54. T. Zhang, Ü. Niinemets, J. Sheffield, J. W. Lichstein, Shifts in tree functional composition amplify the response of forest biomass to climate. *Nature* **556**, 99–102 (2018).
55. Y. Pan, R. Birdsey, J. Hom, K. McCullough, Separating effects of changes in atmospheric composition, climate and land-use on carbon sequestration of U.S. Mid-Atlantic temperate forests. *For. Ecol. Manag.* **259**, 151–164 (2009).
56. C. R. Schwalm *et al.*, Reduction in carbon uptake during turn of the century drought in western North America. *Nat. Geosci.* **5**, 551–556 (2012).
57. M. P. Dannenberg, E. K. Wise, W. K. Smith, Reduced tree growth in the semiarid United States due to asymmetric responses to intensifying precipitation extremes. *Sci. Adv.* **5**, eaaw0667 (2019).
58. P. Ciais *et al.*, Europe-wide reduction in primary productivity caused by the heat and drought in 2003. *Nature* **437**, 529–533 (2005).
59. J. Peñuelas *et al.*, Shifting from a fertilization-dominated to a warming-dominated period. *Nat. Ecol. Evol.* **1**, 1438–1445 (2017).
60. C. Grossiord *et al.*, Plant responses to rising vapor pressure deficit. *New Phytol.* **226**, 1550–1566 (2020).
61. M. E. Dusenge, A. G. Duarte, D. A. Way, Plant carbon metabolism and climate change: Elevated CO_2 and temperature impacts on photosynthesis, photorespiration and respiration. *New Phytol.* **221**, 32–49 (2019).
62. H. Pretzsch *et al.*, Forest growth in Europe shows diverging large regional trends. *Sci. Rep.* **13**, 15373 (2023).
63. G. Murray-Tortarolo *et al.*, A process-model perspective on recent changes in the carbon cycle of North America. *J. Geophys. Res. Biogeosci.* **127**, e2022JG006904 (2022).
64. C. Wu *et al.*, Uncertainty in US forest carbon storage potential due to climate risks. *Nat. Geosci.* **16**, 422–429 (2023).
65. G. Forzieri, V. Dakos, N. G. McDowell, A. Ramdane, A. Cescatti, Emerging signals of declining forest resilience under climate change. *Nature* **608**, 534–539 (2022).
66. E. Burrill *et al.*, "The forest inventory and analysis database: Database description and user guide version 9.0.1 for phase 2" (US Department of Agriculture, Forest Service, 2023), p. 1066. available at web address: https://www.fia.fs.usda.gov/library/database-documentation/index.
67. J. C. Jenkins, D. C. Chojnacky, L. S. Heath, R. A. Birdsey, National scale biomass estimators for United States tree species. *For. Sci.* **49**, 12–35 (2003).
68. C. W. Woodall, L. S. Heath, G. M. Domke, M. C. Nichols, "Methods and equations for estimating aboveground volume, biomass, and carbon for trees in the US forest inventory, 2010" *Gen Tech Rep NRS-88 Newtown Sq. PA US Dep. Agric. For. Serv. North. Res. Stn.* vol. **30** (2011).
69. J. W. Lichstein, C. Wirth, H. S. Horn, S. W. Pacala, "Biomass chronosequences of United States forests: Implications for carbon storage and forest management" in *Old-Growth Forests: Function, Fate and Value*, C. Wirth, G. Gleixner, M. Heimann, Eds. (Springer, Berlin Heidelberg, 2009), pp. 301–341.
70. D. A. Clark *et al.*, Measuring net primary production in forests: Concepts and field methods. *Ecol. Appl.* **11**, 356–370 (2001).
71. P. C. Van Deusen, T. R. Dell, C. E. Thomas, Volume growth estimation from permanent horizontal points. *For. Sci.* **32**, 415–422 (1986).
72. T. W. Beers, C. I. Miller, *Point Sampling: Research Results, Theory, and Applications* (Purdue University Agricultural Experiment Station, 1964).
73. K. Zhu, J. Zhang, S. Niu, C. Chu, Y. Luo, Limits to growth of forest biomass carbon sink under climate change. *Nat. Commun.* **9**, 2709 (2018).
74. M. Uriarte, C. D. Canham, J. Thompson, J. K. Zimmerman, A neighborhood analysis of tree growth and survival in a hurricane-driven tropical forest. *Ecol. Monogr.* **74**, 591–614 (2004).
75. D. M. Bates, J. M. Chambers "Nonlinear models" in *Statistical Models in S* (Routledge, 1992), pp. 421–453.
76. R Development Core Team, R: A language and environment for statistical computing (2022), https://www.r-project.org/ version 4.1.2 (The R Foundation for Statistical Computing, 17 February 2023).
77. J. Pinheiro *et al.*, Package 'nlme'. *Linear Nonlinear Mix. Eff. Models Version* **3**, 274 (2017).
78. M. Plummer, "JAGS: A program for analysis of Bayesian graphical models using Gibbs sampling" in *Proceedings of the 3rd International Workshop on Distributed Statistical Computing*, Vienna, Austria (2003), pp. 1–10.
79. J. Hartung, G. Knapp, S. K. Bimal, "Methods of combining effect sizes" in *Statistical Meta-Analysis with Applications,* D. J. Balding, N. A. C. Cressie, G. M. Fitzmaurice, I. M. Johnstone, G. Molenberghs, D. W. Scott, A. F. M. Smith, R. S. Tsay, S. Weisberg, Eds. (John Wiley & Sons Ltd., 2008), pp. 35–41.
80. W. C. Palmer "Meteorological drought, Research paper no. 45" (U.S. Department of Commerce, National Oceanic and Atmospheric Administration, 1965).
81. PRISM Climate Group, Oregon State University, PRISM Gridded Climate Data, https://prism.oregonstate.edu/ (March 3, 2023).
82. J. T. Abatzoglou, D. J. McEvoy, K. T. Redmond, The west wide drought tracker: Drought monitoring at fine spatial scales. *Bull. Am. Meteorol. Soc.* **98**, 1815–1820 (2017).
83. U.S. Department of Agriculture, Forest Service, Northern Research Station, Forest Inventory and Analysis *Database*, https://apps.fs.usda.gov/fia/datamart/datamart.html (November 1, 2022)
84. West Wide Drought Tracker, *PRISM* Palmer Drought Severity Index, https://wrcc.dri.edu/wwdt/data/PRISM/pdsi/ (August 8, 2022).
85. J. A. Hogan, Quantifying changes in the *dynamics* of U.S. forests using national forest inventory data, https://github.com/hoganhaben/FIA-forest-dynamics (August 29, 2023).